Vladimir Keilis-Borok

Annu. Rev. Earth Planet. Sci. 2002. 30:1–33
DOI: 10.1146/annurev.earth.30.100301.083856

EARTHQUAKE PREDICTION: State-of-the-Art and Emerging Possibilities

Vladimir Keilis-Borok[1,2]
[1]*International Institute of Earthquake Prediction Theory and Mathematical Geophysics, Russian Academy of Sciences, Warshavskoe sh. 79, korp. 2, 113556 Moscow, Russia*
[2]*Institute of Geophysics and Planetary Physics and Department of Earth and Space Sciences, University of California, Los Angeles, California 90095-1567;*
e-mail: vkb@ess.ucla.edu, vkborok@mitp.ru

Key Words earthquake preparedness, complexity, critical transitions, premonitory seismicity patterns

FOREWORD

1. Earthquake prediction is pivotal both for reduction of the damage from earthquakes and for fundamental understanding of lithosphere dynamics. That twofold goal, usual for prediction research, brings up the key questions considered here: (*a*) What predictions are already possible? (*b*) How can damage from earthquakes be reduced on the basis of such predictions, given their limited accuracy? (*c*) What fundamental knowledge has been gained in earthquake prediction research? The common underlying question is, what comes next?
2. This problem is of urgent practical importance because earthquakes pose a rapidly growing threat to survival and sustainable development of our civilization. This is due to the well-known interrelated developments: proliferation of radioactive waste disposals, high dams, nuclear power plants, lifelines, and other objects whose damage poses an unacceptable risk; self-destruction of megacities; destabilization of the environment; and growing socio-economic volatility of the global village. For all of these reasons, seismic risk has escalated also in numerous regions of low seismicity. Today, a single earthquake may take up to a million lives, cause material damage up to $\$10^{12}$, raze a megacity, trigger a global economic depression, render a large territory uninhabitable, and destabilize the military balance in a region.

Earthquake prediction is necessary to undertake disaster preparedness measures, reducing the damage from the earthquakes. This requires that the accuracy of prediction be known, but, contrary to common belief, a timely prediction of low accuracy may be very useful.

3. Earthquake prediction is necessary also for fundamental understanding of the dynamics of the lithosphere, particularly in the timescales of 10^2 years and less. So far, this problem is in the same stage as the theory of gravity was between T. Brahe and J. Kepler: the study of heuristic regularities that are necessary to develop a fundamental theory.
4. Here we review the research that extends to formally defined prediction algorithms and to their tests by advance prediction. Being a part of much broader efforts in earthquake prediction, this is presently most essential both for damage reduction and for understanding the lithosphere. Methodologically, this research integrates theoretical modeling and analysis of observations.
5. Why was this topic suggested for the prefatory chapter of the *Annual Review of Earth and Planetary Sciences*? First, as the reader will see, the earthquake prediction problem is connected, one way or another, with most of the solid Earth sciences, tying together an immense variety of fields and processes in the wide range of time- and space scales. Algorithmic prediction, if successful, provides one of the major hopes for bringing internal order in that diversity of topics and methods. Indeed, since the times of Galileo, if not through the whole history of science, prediction has been a major tool of fundamental research, a source of heuristic constraints and hypotheses, and the final test of theories.

Second, the earthquake prediction problem happens to be closely relevant to what I believe is a current frontier of the solid Earth sciences: emergence of a fundamental concept that would succeed plate tectonics, provide a fundamental base for prediction and (with luck) control of geological and geotechnical disasters, and establish links with "universal" scenarios of critical transitions in nonlinear (complex) systems.
6. The earthquake prediction realm still exhibits a striking gap in mutual awareness. This gap is amazingly large even for such a huge conglomerate of problems and professions; for earthquake preparedness it bodes ill—the chance to undertake preparedness measures should not be missed.
7. This gap might be partly due to the lack of a common language. To reach a possibly wider audience, I wrote this review in qualitative terms (retaining, I hope, a reasonable precision), although the studies considered here are entirely quantitative, with a substantial (to put it gently) mathematical component.
8. The following topics are covered by this review. (*a*) Structure of the earthquake-prone fault network: hierarchy of blocks and faults, and nucleation of earthquakes in mosaic nodes at the faults' intersections and junctions. (*b*) Fault networks as a stockpile of instability: a multitude of mechanisms that destabilize the strength-stress field and turn the network into a complex system with earthquakes for critical phenomena and the predictability of that system. (*c*) Prediction algorithms: premonitory seismicity patterns and the performance of the algorithms in advance prediction worldwide. (*d*) Error diagrams—a tool for validation of prediction methods. (*e*) Four paradigms in earthquake prediction: basic types of precursors,

long-range correlations in the fault network, partial similarity of precursors worldwide, and their dual origin—some precursors are common for many complex systems, others are Earth-specific. (*f*) Earthquake prediction and earthquake preparedness. (*g*) Emerging possibilities, yet unexplored.

9. This paper is a preview to the monographic treatise on earthquake prediction, now in preparation, by a team from the International Institute of Earthquake Prediction Theory and Mathematical Geophysics, Russian Academy of Sciences. Most of the specific findings discussed here were obtained in that Institute as well as in the following institutions: in France, the Institute of the Physics of the Earth (Paris) and Observatory of Nice; in the United States, Cornell and Purdue Universities, University of California, Los Angeles, University of Southern California, Massachussetts Institute of Technology, and U.S. Geological Survey; in Italy, the Abdus Salam International Center for Theoretical Physics, Universities of Rome ("La Sapienza") and Trieste.

INTRODUCTION

Seismicity and Geotectonics

Earthquakes occur in some parts of the outer shell of the solid Earth, called the lithosphere; its thickness ranges from a few kilometers near the mid-ocean ridges to a few hundred kilometers in certain continental regions. Below the lithosphere, down to a depth of 2900 km, lies Earth's mantle, which is partially melted in its upper 10^2 km.

Large-scale convection currents in the mantle, with characteristic velocities of centimeters per year, and internal processes within the lithosphere itself put the lithosphere in a state of permanent motion, highly irregular in space and time. Two major distinctive features of the lithosphere are responsible for the generation of earthquakes: (*a*) It is subject to fracturing. Exceptions are the soft soil at its very top, and the lower depths where a combination of stress, strength, and temperature is unfavorable for fracturing. (*b*) It is hierarchically divided into volumes ("blocks") driven by tectonic forces; they move relative to each other along the faults that separate them. In seismically active regions, earthquakes produce a significant part of the relative motion of the blocks. This makes seismicity an indelible component of the tectonic development of Earth.

An earthquake starts as an episode of rupture and discontinuous displacement in a certain part of a fault system, which becomes an earthquake source. These episodes alternate with slower deformations in the "stick-slip" sequences. Nearly a million earthquakes with magnitude 2 or more are registered each year worldwide. About a hundred of them cause considerable damage and once or twice in a decade a catastrophic earthquake occurs. Worldwide distribution of seismicity is shown in Figure 1. Epicenters of earthquakes are concentrated in seismic belts, encompassing tectonic plates—the major blocks comprising the lithosphere.

Stages of Prediction

Due to the multiscale nature and complexity of the processes expressed in seismicity, the problem of earthquake prediction consists of a consecutive step-by-step narrowing down of the time-space domain where a strong earthquake should be expected. Five major stages of earthquake prediction are commonly distinguished. The background stage provides "territorial" distribution of the recurrence time for destructive earthquakes of different magnitudes, up to the maximal possible one. The subsequent stages, fuzzily divided, include time-prediction; they differ in characteristic duration of alarms—the time intervals, where an earthquake is predicted (these intervals are indicated in brackets below): long-term (tens of years), intermediate-term (years), short-term (months to weeks), and immediate (days and less).

Data

The problem of earthquake prediction is particularly challenging because the bulk of the earthquake-prone lithosphere is inaccessible for the direct measurement of earthquake-related stress and strength fields. The lithosphere is virtually a black box in a state of permanent activity. It generates a multitude of observable time-dependent fields, which provide potential data sources for earthquake prediction. Prediction algorithms reviewed here diagnose the approach of a strong earthquake by analysis of one of such fields—seismic activity in a wide magnitude range.

FAULT NETWORK: HIERARCHICAL STRUCTURE

Almost all earthquakes occur in the fault network, delineating the major structural elements of the lithosphere (Keilis-Borok 1990a, Turcotte 1997): a hierarchy of blocks separated by boundary zones, with densely fractured nodes at junctions and intersections of these zones.

Blocks

The lithosphere is divided into a hierarchy of volumes, or blocks, that move relative to each other. The largest blocks are ten or so major tectonic plates of continental size. They include smaller blocks such as shields or mountain belts. After 15 to 20 consecutive divisions, we come to nearly 10^{25} grains of rocks.

Boundary Zones

The blocks are separated by less rigid boundary zones, whose widths are 10–100 times smaller than the characteristic dimension of the blocks that they separate. The zones between the largest blocks are known as fault zones (10^2–10^1 km), then as faults (km to tens of meters), sliding surfaces (meters to centimeters),

and, finally, as interfaces between the grains of rocks. Except at the lowest levels of hierarchy, each boundary zone has a similar hierarchical structure with more dense division: It consists of its own blocks, divided by boundary zones, etc. For brevity, we refer to all boundary zones as faults, unless distinction is necessary.

Nodes

Even more densely fractured mosaic structures, called nodes, are formed around the intersections and junctions of the faults. Their origin is due, roughly, to collision of the corners of the blocks (Gabrielov et al. 1996, King 1983). The formalized definition of nodes is developed by Alekseevskaya et al. (1977).

Nodes are well known in structural geology and geomorphology and play a prominent textbook role in geological prospecting as attractors of mineral deposits. Their origin and strong impact on seismicity, sometimes overlooked in earthquake studies, are discussed below in the section Geometric Instability. The systems of boundary zones and nodes are called here the fault networks.

FAULT NETWORK: THE STOCKPILE OF INSTABILITY

The boundary layers of different rank, from the Circum Pacific seismic belt, with the giant triple junctions for the nodes, to an interface between the grains of rocks, with the corners of the grains for the nodes, play a similar role in lithosphere dynamics. Specifically, although tectonic energy is stored in the whole volume of the lithosphere and well beneath, the tectonic energy release (through earthquakes and slow deformations) is to a large extent controlled by the processes in the relatively thin fault networks. This disparity is due to the following reasons.

First, as in any solid body, deformations and fracturing in the lithosphere are controlled by the {stress-strength} field. At the same time, the strength of the fault network is weakened by denser fragmentation and higher permeability to fluids (compared to the blocks). For that reason, tectonic deformations, earthquakes included, are concentrated in the fault networks, whereas the blocks move more as a whole, with smaller internal deformations. In the timescale most relevant to the earthquake prediction problem, tens of years or less, a major part of lithosphere dynamics is realized through the deformation of the fault networks and relative movement of the blocks.

Second, the strength of the fault networks is not only smaller but also highly unstable, since it is sensitive to many processes there. Two types of instability coexist in the fault network: “physical,” originated by a physical or chemical mechanism at the elementary (micro) level, and “geometric,” controlled by the geometry of the fault network on a global (macro) level.

Physical Instability

The simplest source of instability is the abrupt triggering of an earthquake when the stress exceeds the strength on some segment of a fault. Some other sources of physical instability are described below.

RHEBINDER EFFECT, OR STRESS CORROSION

Description Many solid substances lose their strength when they come in contact with certain surface-active liquids. The liquid diminishes the surface tension and, consequently, the strength. When the strength drops, cracks may appear under a small stress, even gravitational stress might suffice. This triggers expansion of fatigue: Liquid penetrates the cracks and they grow, with liquid propelling forward until it dissipates. This mechanism, called the Rhebinder effect (Gabrielov & Keilis-Borok 1983), requires very little energy to generate fracturing. It was discovered first for metals and ceramics. Then, such combinations of solid substances and surface-active liquids were recognized among the common ingredients of the lithosphere, e.g., a basalt and sulphur solution. When they meet, a grid of cracks permeates the basalt, and the efficient strength may instantly drop by a factor 10 or more. Thus, the Rhebinder effect brings into the dynamics of the lithosphere a strong and specific instability controlled by the stress field and by the geochemistry of the fluids.

Relevance to prediction The weakened areas, where the cracks concentrate, may have only certain configurations, depending on singularities of the stress field. Examples of such configurations are shown in Figure 2. The thin lines show trajectories or cracks. Each heavy line is a separatrix, dividing different patterns of the cracks.

How would an observer of the lithosphere interpret Figure 2? Suppose the source of a fluid appears in the place shown by the arrows. It will concentrate in the shaded areas and their strength will drop. A slight displacement of the source across a separatrix may divert the fatigue to a different place and completely change its configuration.

This effect might explain many phenomena highly relevant to the development of a strong earthquake. For example, the diagrams show formation of weak links (four top panels) and asperities (two bottom panels). However, such explanations have at least two limitations. First, configurations shown in Figure 2 are the local ones. Inhomogeneity of stress and strength fields and dissipation of fluids may prevent their formation in the scale of the observed premonitory patterns, which is up to hundreds of kilometers. More likely, these configurations are the elements that compose a nonlocal infrastructure of fatigue. Second, the Rhebinder effect is not a single mechanism of physical instability. Even the fluids alone may generate other equally strong mechanisms, such as the one described below.

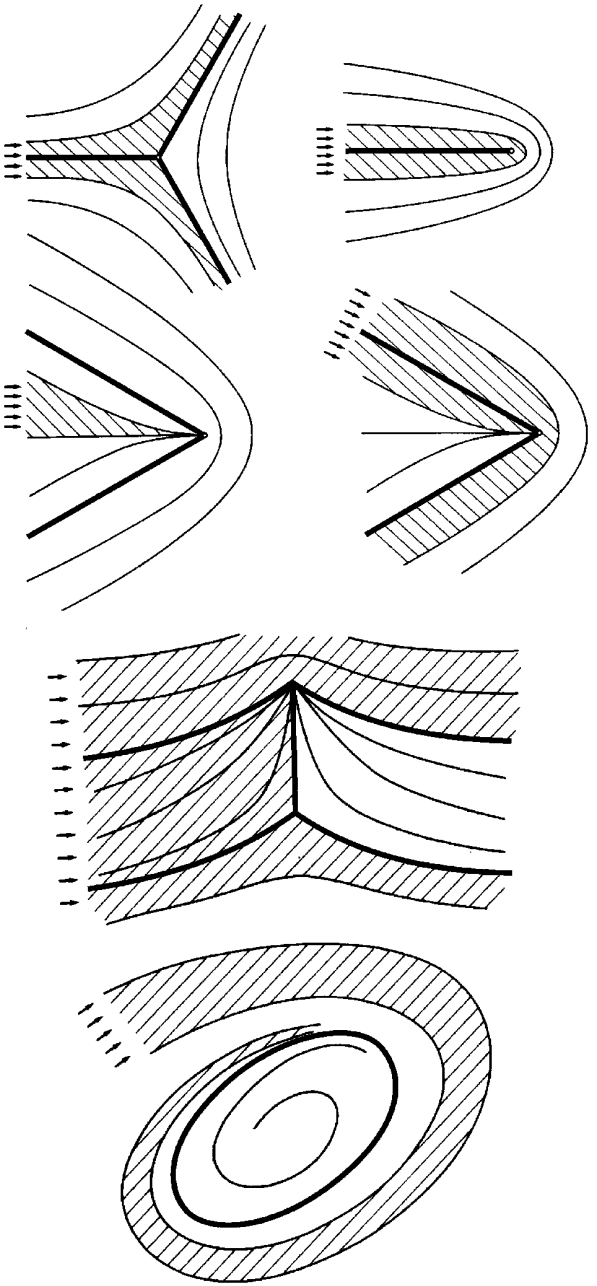

Figure 2 Instability caused by stress corrosion. Geometry of the weakened areas depends on the type of stress field's singularity and on direction from which the fluid arrives; see further explanations in the text. After Gabrielov & Keilis-Borok 1983.

NONLINEAR FILTRATION

Description One of the competing mechanisms is filtration of the fluids through the fault zones. Barenblatt et al. (1983) modeled this process as the relative movement of impermeable blocks separated by a porous layer. The latter is connected with a source of a fluid that migrates along the gradient of pressure. The fluid acts as the lubricator, decreasing the friction and triggering the episodes of fast movements—the "slips." If porosity is subcritical (below a certain threshold) the slip, once started, will increase the friction and self-decelerate. At most, the fluid will trigger vacillating creep or a slow earthquake. However, if porosity exceeds a critical threshold, the slip will decrease the friction and the continuously forming microcracks will self-accelerate, grow, and merge at an escalating rate.

The porosity can be raised above the critical threshold by infiltration of a fluid itself; this will increase the tension and the pores will expand. Critical porosity propagates along the fault zone with finite velocity comparable at an observed velocity of migration of seismicity.

Relevance to prediction Nonlinear filtration also explains many features of real seismicity, including the premonitory rise of seismic activity and of earthquake clustering. Moreover, it implies certain premonitory changes in the dynamics of fluid and electromagnetic field. However, the same limitations hold as in the case of stress corrosion. First, such instabilities may rise simultaneously within boundary zones of different rank and interact along the hierarchy, creating more complex patterns of filtration-generated instability. And second, this is not a single major source of physical instability.

OTHER MECHANISMS Further examples illustrate the diversity of mechanisms, causing the physical instability of fault networks.

"***Fingers of fluids***" These fingers spring out at the front of the fluid, migrating in a porous medium.

Dissolution of rocks Its impact is magnified by the Riecke effect—increase of solubility of rocks with pressure. This effect leads to a mass transfer: Solid material is dissolved under high stress and carried out in solution along the stress gradient to areas of smaller stress where it precipitates.

Petrochemical transitions Some petrochemical transitions tie up or release the fluids, as in formation or decomposition of serpentines, respectively. Others cause a rapid drop of density, such as in transformation of calcite into aragonite. This would create a vacuum and unlock the fault; the vacuum will be closed at once by hydrostatic pressure, but the rupture might be triggered.

Sensitivity of dynamic friction The sensitivity of dynamic friction to the local physical environment is another mechanism causing instability of the fault networks.

Mechanical processes Several mechanical processes, such as multiple fracturing, buckling, viscous flow, etc., contribute to the instability of the fault networks.

Impact of pressure and temperature The above mechanisms are also influenced by pressure and temperature.

This list is by no means complete. With such a diversity of mechanisms, physical instability of the fault network can hardly be attributed to any single mechanism alone.

Geometric Instability

The geometry of the fault network is often incompatible with tectonic movements. This leads to accumulation of stress, deformation, fracturing, and change of the fault geometry, jointly destabilizing the fault network. Two integral measures of that instability have been found by Gabrielov et al. (1996): (*a*) geometric incompatibility, concentrated in mosaic nodes, and (*b*) kinematic incompatibility spread over the whole lithosphere, including the blocks. Each measure estimates an integrated effect of tectonic movements in a wide range of timescales, from seismicity to neotectonics.

GEOMETRIC INCOMPATIBILITY

Description The phenomenon of geometric incompatibility is illustrated in Figure 3. It shows an intersection of two strike-slip faults separating the moving blocks. If the movements indicated by the arrows on Figure 3*a* could continue, the corners *A* and *C* would penetrate into each other and an intersection point would split into a parallelogram (Figure 3*b*). In reality, such a parallegram cannot be formed; instead, collision of the corners will trigger accumulation of stress and deformations near the intersection, followed by the fracturing and change of the fault geometry. Geometric incompatibility is a quantitative measure of this process. If the corners of the blocks tend to overlap (Figure 3*a*,*b*), the ensuing compression locks up the intersection. If all the corners tend to diverge (Figure 3*c*,*d*), the ensuing tension will unlock the intersection.

Formation of the nodes Accumulation of stress at the corners of tectonic blocks was first described by McKenzie & Morgan (1969) for a triple junction. They found a condition under which a single junction "can retain its geometry as the plates move" so that the stress will not accumulate. King (1983) suggested that in a general case, when that condition is not satisfied, the ensuing fracturing will not dissolve the stress accumulation, but will only redistribute it among newly formed corners. As a result, a hierarchy of progressively smaller and smaller faults is formed around an initial intersection; this is a node, recognizable by its densely mosaic structure, probably having self-similar fractal geometry.

Stokes-type theorem In reality, we encounter not a single intersection, as in Figure 3, but clusters of intersections in a node, and interacting nodes in a fault

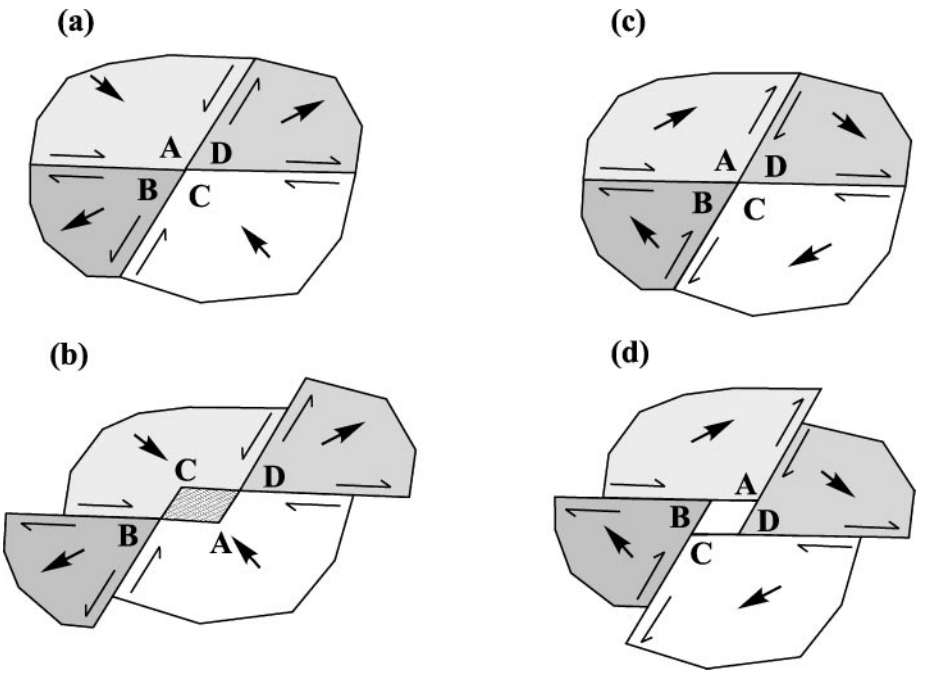

Figure 3 Geometric incompatibility near a single intersection of faults. *a*, *c*—initial position of the blocks; *b*, *d*—physically unrealizable extrapolation of initial movement. *a*, *b*—locked node; *c*, *d*—unlocked node. After Gabrielov et al. 1996.

network. Luckily, geometric incompatibility is additive. Gabrielov et al. (1996) found the analog of the Stokes theorem connecting the total geometric incompatibility of a fault network within a boundary with observations on that boundary. This allows one to estimate from outside geometric incompatibility in a complicated structure, such as an ensemble of nodes. This theorem reflects the fact that geometric incompatibility in different nodes is interdependent because the nodes are connected through the movements of blocks and on the faults. A strong earthquake in a node might change its incompatibility, thus affecting the generation of earthquakes in other nodes.

Such interplay is described by Prozorov & Shreider (1990). They observed that a strong earthquake is followed by "long-range aftershocks;" a rise of seismic activity in the area where the next strong earthquake is going to occur within 10 years or so.

Earthquakes nucleation There is compelling evidence that strong earthquakes nucleate within the nodes, or more precisely, within certain specific nodes that can be recognized by geological and geomorphologic criteria (Gelfand et al. 1976).

Such nodes have been mapped for many regions with different level of seismicity, from the Pyrenees, the Alps, and the Caucasus to California, the Himalayas, and the South American Andes. That analysis was well validated by the occurrence of strong earthquakes after publication of the maps (Gorshkov et al. 2001).

KINEMATIC INCOMPATIBILITY Let us apply to the lithosphere the well-known Saint Venant condition of kinematic compatibility (McKenzie & Parker 1967). It ensures that the relative movements on the faults can be realized through the absolute movements of the blocks separated by the faults. Kinematic incompatibility is a measure of deviation from that condition.

Kinematic incompatibility is also additive, its values in different parts of the fault network can be summed up, and the total kinematic incompatibility in a region is connected with observations on its boundary by an analog of the Stokes theorem (Gabrielov et al. 1996).

Conclusion: Complexity and Critical Phenomena

Summing up, the dynamics of the lithosphere is controlled by a wide variety of mutually dependent mechanisms, to a large extent concentrated in the fault network and interacting across and along its hierarchy. Each mechanism creates strong instability of the {strength-stress} field, particularly of the strength. Except under very special circumstances, no single mechanism prevails so that the others can be neglected.

Even the primary element of the lithosphere—a grain of a rock—may act simultaneously as a material point; a visco-elastic body; an aggregate of crystals; and a source or absorber of energy, fluids, and volume. Moreover, its body and surface are involved in quite different processes.

To assemble the set of corresponding equations is unrealistic and probably impossible: a maxim in nonlinear dynamics tells "one cannot understand a chaotic system by breaking it apart" (Crutchfield et al. 1986). Rather, one may hope for a generalized theory (or at least a model) that directly represents the gross integrated behavior of the lithosphere. That brings us to the concept that ". . . in the timescale relevant to earthquake prediction problem, 10^2 years and less, the mechanisms destabilizing the strength of the fault network turn the lithosphere into a nonlinear hierarchical dissipative system" (Keilis-Borok 1990a). Strong earthquakes are critical phenomena in that system (Sornette & Sammis 1995, Turcotte 1997, Sornette 2000, Rundle et al. 2000).

Complex systems are not predictable with absolute precision. However, after a coarse-graining (i.e., averaging), in a not-too-detailed scale, premonitory phenomena emerge and a system becomes predictable, up to the limits (e.g., Gell-Mann 1994, Holland 1995). Accordingly, prediction of complex systems requires a holistic approach, "from the whole to details," in consecutive approximations, starting with the most robust coarse-graining of the processes considered.

GENERAL SCHEME OF PREDICTION

An Early Example

The first prediction algorithm of the type considered here was introduced by Keilis-Borok & Malinovskaya (1964). Prediction of a strong earthquake was based on the rise of seismic activity in the medium magnitude range. The total area of rupture surfaces in the earthquake sources was chosen as a measure of seismic activity defined by the function

$$\Sigma(t) = \sum_i 10^{Bm_i}, \quad m_i < M. \tag{1}$$

Here, m_i is the magnitude of i-th earthquake (a logarithmic measure of energy release) and M is the magnitude of a strong earthquake targeted for prediction. Summation is taken over the earthquakes that occurred within the sliding time window $(t - s, t)$ in the region considered. The value of parameter B was chosen from condition that each term under summation is coarsely proportional to the rupture area in a source.

The premonitory seismicity pattern Σ was diagnosed by the condition $\Sigma(t) \geq C_\Sigma$. The threshold C_Σ is self-adapting to a target magnitude M; it is proportional to the rupture area in the source of a single strong earthquake. The emergence of pattern Σ before 20 strong earthquakes worldwide was demonstrated by Keilis-Borok & Malinovskaya (1964). Figure 4 shows an example for the catastrophic in Assam earthquake in India in 1950, M = 8.6.

Figure 4 Illustration of the premonitory seismicity pattern Σ: rise of the functional $\Sigma(t)$ before the Assam earthquake in India (1950, M = 8.6). Dotted line shows the threshold C_Σ defining this pattern. After Keilis-Borok & Malinovskaya 1964.

Pattern Σ was the first premonitory seismicity pattern that demonstrated the major features of the patterns discovered later: long-range correlations and similarity (see Four Paradigms below).

Formulation of the Problem

We consider prediction as a pattern recognition problem: Given is the dynamics of seismicity (and/or other relevant fields) in a certain area prior to a moment t; to predict whether a strong earthquake will or will not occur within that area during the subsequent time interval $(t, t + \Delta)$; note that prediction may include reduction of the area.

In terms of pattern recognition, the "object of recognition" is a moment t. The problem is to recognize whether or not it belongs to the time interval Δ preceding a strong earthquake. That interval was named *TIP*, for the time of increased probability of a strong earthquake.

Pattern recognition of infrequent events (Gelfand et al. 1976, Keilis-Borok & Press 1980) happens to be very efficient in such an approach to prediction. That methodology has been developed by the school of I. Gelfand for the study of rare phenomena of highly complex origin, a situation where classical statistical methods are inapplicable.

The probabilistic side of prediction is reflected in the rates of its errors.

Data Analysis

Under the approach described above, the data analysis comprises the following steps:

(*a*) A sequence of earthquakes is robustly described by the functionals $F_k(t)$, $k = 1, 2, \ldots$, each depicting a certain premonitory seismicity pattern (Figure 5). With a few exceptions, the functions are defined in a sliding time window $(t - s, t)$; the value of a function is attributed to the end of the window.

(*b*) Emergence of a premonitory seismicity pattern is defined by the condition

$$F_k(t) \geq C_k. \tag{2}$$

The threshold C_k is usually defined as a certain percentile of the functional F_k.

(*c*) An alarm is triggered when a single pattern or a certain combination of patterns emerges; different patterns are used in different algorithms (see Prediction). An alarm lasts for a certain time period; in some algorithms, it is terminated if and when the strong earthquake occurs. The possible outcomes of prediction are illustrated in Figure 6.

This scheme is open for the use of other data, not necessarily seismological ones. The key element in development of such an algorithm is obviously to find the functionals $F_k(t)$ that provide a good prediction.

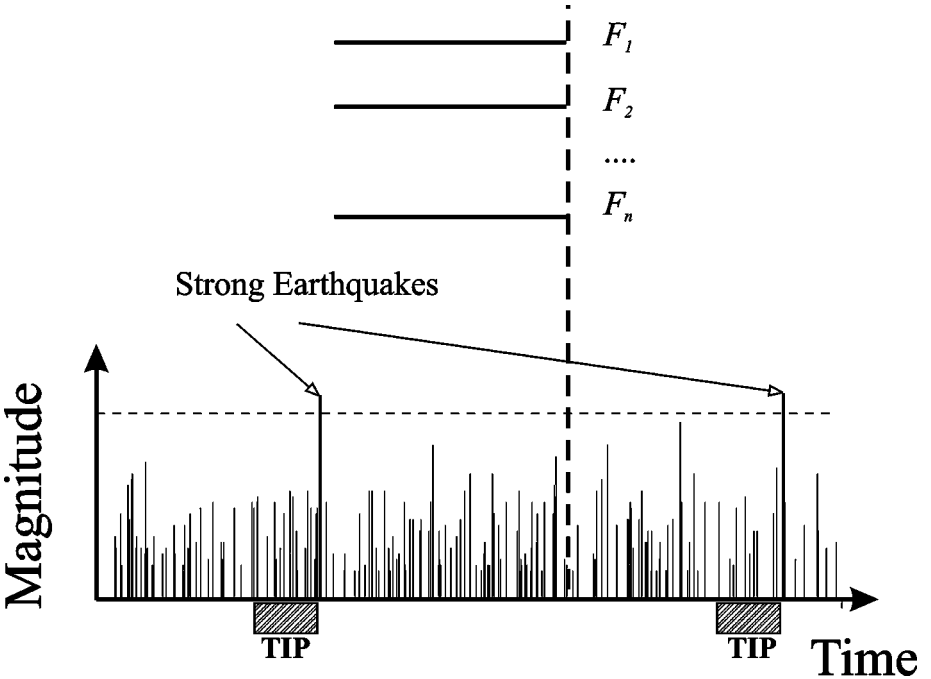

Figure 5 General scheme of prediction. See explanations in the text. After Keilis-Borok 1990a.

Error Diagrams

Error diagrams introduced in seismology by Molchan (1997) show the trade-off between different errors of prediction. They are pivotal in the development and validation of prediction methods, as well as in using predictions for enhancing earthquake preparedness.

DEFINITION Consider a prediction algorithm applied to a certain territory during the time period T. A certain number A of alarms is declared and A_f of them

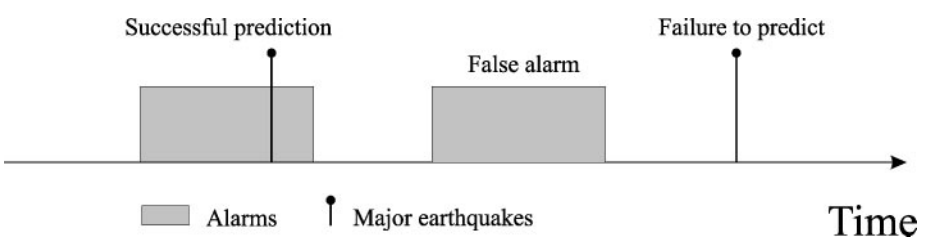

Figure 6 Possible outcomes of prediction.

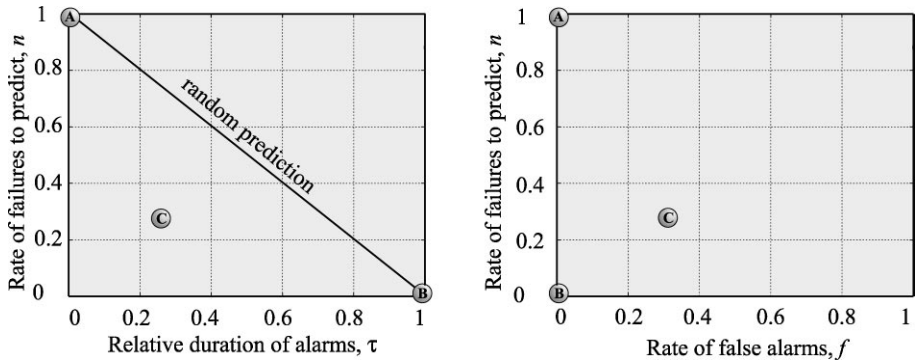

Figure 7 Scheme of the error diagram (Molchan, 1997). Points *A*, *B*, and *C* show performance of a prediction method: the trade-off between the rate of false alarms, f; the rate of failures to predict, n; and the relative time-space occupied by alarms, τ. Points on the diagonal on the left plot correspond to a random guess. Point *A* corresponds to the trivial "optimistic" strategy, when an alarm is never declared; point *B* to the trivial "pessimistic" strategy, when an alarm takes place all the time; point *C* to the realistic prediction. See text for more details.

happened to be false. N strong earthquakes occurred, and N_f of them have been missed by alarms. Altogether, the alarms cover the time D. Performance of the algorithm is characterized by three dimensionless parameters: the total relative duration of alarms, $\tau = D/T$; the rate of failures to predict, $n = N_f/N$; and the rate of false alarms, $f = A_f/A$.

The values of τ, n, and f are summed up on an error diagram, schematically illustrated in Figure 7. Different points correspond to different combinations of adjustable elements.

To validate an algorithm, an exhaustive set of numerical experiments is designed (e.g., Gelfand et al. 1976); they take a lion's share of effort in the development of an algorithm. A prediction algorithm makes sense only if its performance is (*a*) sufficiently better than a random guess, and (*b*) not too sensitive to variation of adjustable elements. An error diagram is a powerful tool for checking these conditions.

FOUR PARADIGMS

Summarizing the previous section, we discern consecutive milestones in the development of a prediction method.

(*a*) Hypothetical premonitory phenomenon; in the case of pattern Σ, it is a rise of the seismic activity.

(*b*) Qualitative definition of a seismicity pattern capturing that phenomenon. In the case of pattern Σ, it is large area unlocked by the earthquakes in a medium magnitude range. That phenomenon may also be captured by

other patterns; for example, by the number of earthquakes, not weighted by magnitude.

(*c*) The formal quantitative definition of that pattern by a functional defined on an earthquake sequence; this is $\Sigma(t)$ in the case of pattern Σ and $F_k(t)$ in the general scheme of prediction (see Figure 5).

(*d*) The prediction algorithm based on such functionals or on their combinations (see Data Analysis above).

The paradigms formulated here provide orientation for research in these directions. They have been found in the quest for premonitory seismicity patterns in the observed and modeled seismicity. There are compelling reasons to also apply them to premonitory phenomena in other relevant fields. An overview of seismicity patterns and prediction algorithms is given in the two subsequent sections.

Paradigm I. Basic Types of Premonitory Phenomena

The approach of a strong earthquake is indicated by the following phenomena, reflecting the changes in the basic characteristics of seismicity: (*a*) rise of seismic activity, (*b*) rise of earthquake clustering in space and time, (*c*) rise of the earthquakes' correlation range, (*d*) transformation of frequency—magnitude relation, (*e*) rise of irregularity in space and time, (*f*) reversal of territorial distribution of seismicity, (*g*) rise of correlation between different components (decrease of dimensionality, and (*h*) rise of response to excitation.

The place of premonitory phenomena in the general scheme of earthquake prediction is discussed at the beginning of this section. The essence of these phenomena is illustrated in the next section by specific seismicity patterns that capture them. Here, we give just a few explanations to make the description of this paradigm self-sustaining. Seismic activity (*a*) is the rate of earthquake occurrence; earthquake clustering (*b*) is the tendency of the earthquakes to occur closely in time and space; earthquakes' correlation range (*c*) is the distance within which the earthquakes do not occur independently; transformation of the frequency magnitude relation (*d*) favors relatively stronger earthquakes (see Figure 10); reversal of territorial distribution of seismicity (*f*) consists of the rise of activity in the areas, where average activity is relatively low, and vice versa; for the last two phenomena, (*g*) and (*h*), we so far have only the common general definitions not yet specified for the problem considered.

HOW THESE PHENOMENA HAVE BEEN FOUND Premonitory seismicity patterns of the first two types, (*a*) and (*b*), have been found first in the observations, and then in the models (Keilis-Borok 1990b, Keilis-Borok & Shebalin 1999, Gabrielov et al. 2000); patterns of the next three types, (*c*)–(*e*), have been found in the reverse order, first on the models (Gabrielov et al. 2000, Newman et al. 1995, Sornette 2000), and then in observations; reversal of territorial distribution of seismicity (*f*) has been found in observations (Shebalin & Keilis-Borok 1999) and is not explored on the

models yet; the last two phenomena remain purely hypothetical. Patterns of the first two types—rise of intensity and clustering—have been validated by statistically significant predictions of real earthquakes (Molchan et al. 1990, Keilis-Borok & Shebalin 1999).

Paradigm II. Long-Range Correlations

The generation of an earthquake is not localized around its future source. A sequence of earthquakes is generated by a fault network, rather than each earthquake being generated by a segment of a single fault. Accordingly, the premonitory signals of an approaching earthquake come not only from a narrow vicinity of the incipient source but from a much wider area.

SIZE OF THE AREAS WHERE PREMONITORY PHENOMENA ARE FORMED Let M be the magnitude of a strong earthquake, and $L(M)$ the characteristic length of its source. At the intermediate-term stage of prediction (in the timescale of years), premonitory phenomena may be formed within distance $10L(M)$ from the source; it might be reduced down to $3L–L$ in a second approximation (Kossobokov et al. 1990). At the long-term stage, in the timescale of tens of years, that distance reaches approximately 100 L. For example, according to Press & Allen (1995), the Parkfield, CA, earthquake, with M close to 6, $L \approx 10$ km, "... is not likely to occur until activity picks up in the Great Basin or the Gulf of California," nearly 800 km away.

HISTORICAL PERSPECTIVE An early and probably the first estimation of the area where premonitory patterns are formed was obtained for pattern Σ (See An Early Example). Table 1 shows similar estimations for other intermediate-term patterns. It is noteworthy that Charles Richter, who was generally skeptical about the

TABLE 1 Linear size of the regions, where premonitory phenomena are observed

Size, $d(M)$	Measure/algorithm	Reference[b]
Up to $10L$[a]	Total area of sources	Keilis-Borok & Malinovskaya 1964
$3L–5L$	CN	Keilis-Borok & Rotwain 1990
$5L–10L$	M8	Keilis-Borok & Kossobokov 1990
$L–3L$	M8 & MSc	Kossobokov et al. 1990
$\sim 5L$[c]	Benioff strain release	Bufe & Varnes 1993, Bowman et al. 1998
$\sim 100L$	Seismic activity	Press & Allen 1995

Notes: (*a*) L is the linear size of rupture in the source of an approaching strong earthquake. (*b*) References are given to the recent (known to the authors) publications rather than to original ones. (*c*) The last two rows are related to timescale of tens of years.

feasibility of earthquake prediction, made exception to the pattern Σ specifically because it was based on long-range correlations. He wrote (Richter 1964): " . . . It is important that [the authors] confirm the necessity of considering a very extensive region including the center of the approaching event. It is very rarely true that the major event is preceded by increasing activity in its immediate vicinity."

MECHANISMS OF LONG-RANGE CORRELATIONS To explain the long-range correlations, several mechanisms (not mutually exclusive) have been suggested. They may be divided into two groups.

1. Some explanations attribute long-range correlations to a large-scale process controlling stress and strength in the lithosphere. Among such processes are microrotation of tectonic plates (Press & Allen 1995); interaction of crustal blocks (Soloviev & Vorobieva 1999); microfluctuation in the direction of mantle currents (Keilis-Borok & Shebalin 1999); migration of pore fluids in fault systems (Barenblatt et al. 1983); hydrodynamic waves in the upper mantle, triggering strong earthquakes (Romanowicz 1993); perturbations of the ductile layer beneath the seismically active zone (Aki 1996); inelasticity and inhomogeneity of lithosphere, etc. Such mechanisms would act under different circumstances, separately or jointly. Altogether, they make long-range correlations inevitable.
2. In another approach, the lithosphere is regarded as a nonlinear chaotic or complex system; then the long-range correlations are again inevitable, as a general feature of chaotic systems in a near-critical state (Keilis-Borok 1990a, Turcotte 1997, Newman et al. 1994, Bowman et al. 1998, Rundle et al. 2000, Sornette 2000).

Paradigm III. Similarity

Premonitory phenomena are similar (identical after normalization) in extremely diverse environments and in a broad energy range. The similarity is not unlimited, however, and regional variations of premonitory phenomena do emerge.

Premonitory seismicity patterns happen to retain a prediction power through a large variety of environments: microfractures in laboratory samples; induced seismicity; earthquakes in subduction zones, major strike-slip fault zones, rift zones, and finally platforms (Keilis-Borok & Shebalin 1999). The corresponding seismic energy release ranges from ergs to 10^{25} ergs. However, the performance of prediction algorithms does vary from case to case.

An opportunity to explore, albeit qualitatively, the further frontiers of similarity is provided by registration of the 111 flashes of energy radiated from the neutron star with celestial coordinates 1806–20 (Kossobokov et al. 2000). These flashes are attributed to the "starquakes," i.e., fractures in the neutron star crust. Starquakes and earthquakes originate in exceedingly different environments: Earth's crust is composed of grains of rocks whereas the crust of the neutron star is a lattice of

heavy nuclei; the radius of Earth and the neutron star is 6731 km and 10 km, respectively; density is $5.5 \cdot 10^6$ g/m^3 and 10^{14} g/m^3; energy release during a quake is up to 10^{26} ergs and 10^{46} ergs.

Figure 8 compares the emergence of premonitory patterns before a major starquake and an earthquake in the Aquaba Gulf, on December 11, 1995, M = 7.3. The functionals capturing these patterns are taken from the earthquake prediction algorithms (see Prediction, below): functionals Σ, N, Z, and L capture the intensity of earthquakes flow; B captures the earthquakes' clustering.

The patterns work in both cases, their fantastic difference notwithstanding. Only the timescale for the starquakes had to be readjusted a posteriori.

Paradigm IV. Dual Nature of Premonitory Phenomena

Some of the premonitory phenomena are "universal," common for hierarchical complex nonlinear systems of different origin; others are specific to geometry of the fault network, or to a certain physical mechanism controlling the {strength-stress} field in the lithosphere.

UNIVERSAL PREMONITORY PHENOMENA The known premonitory seismicity patterns happen to be universal in the sense that they emerge in the lattice models, not specific to Earth only; accordingly, one may expect them in systems of quite different origin. Such models are developed in statistical physics and nonlinear dynamics. The most complete set of premonitory seismicity patterns was reproduced by the model of colliding cascades (Gabrielov et al. 2000, Zaliapin et al. 2001). A premonitory increase of correlation range was first found in this model and then, with the same definition, in the observed seismicity.

EARTH-SPECIFIC PREMONITORY PHENOMENA Phenomena of this kind have not yet been defined in a clear-cut way to be incorporated directly in the prediction algorithms. Here we hypothesize what such phenomena might be.

Reversals of geometric incompatibility might produce asperities, relaxation barriers, weakest links, alternation of seismicity, and creep ("loud" and "silent" earthquakes)—phenomena that are highly relevant to prediction. If this conjecture is correct, such phenomena would migrate from node to node with the velocity typical for migration of seismicity: tens to hundreds km/year.

Kinematic incompatibility is relevant to prediction because it captures the stress accumulation in the fault network, blocks included.

PREDICTION

Here we provide an overview of prediction algorithms based on premonitory seismicity patterns. Specifically, we consider algorithms for intermediate-term prediction, which are currently at different stages of validation. There is a large

family of such algorithms, and an even larger one of individual premonitory patterns.

The algorithms considered are based on the same general scheme of data analysis and the same underlying concepts. These common elements are described in previous sections.

Premonitory Seismicity Patterns

Each of the premonitory phenomena listed in Four Paradigms (Paradigm I) is captured by different seismicity patterns described here. These patterns are formed by the earthquakes within a given territory, magnitude range, and time interval; for most of the patterns, aftershocks are eliminated from consideration. Earthquake energy E and size of a seismic source are roughly estimated from the magnitude.

RISE OF SEISMIC ACTIVITY

Total area of seismic sources, or pattern Σ The predictive power of pattern Σ (see An Early Example above) has been demonstrated for many regions of the world (Keilis-Borok & Malinovskaya 1964, Keilis-Borok et al. 1980). The area of a source is assumed to be proportional to $E^{2/3}$.

Active zone size (AZS) The *AZS* captures the size of the area where seismic activity has risen. It was found in a model by Pepke et al. (1994) and then in the observed seismicity of California by Kossobokov & Carlson (1995). That pattern also reflects the premonitory rise of correlation range, discussed below.

Benioff strain release (ε) ε captures the weighted number of earthquakes, with the weights proportional to $E^{1/2}$ (Bowman et al. 1998, Bufe & Varnes 1993). Many recent studies advocate a power growth of the cumulative Benioff strain release prior to a strong earthquake.

Number of earthquakes (N) N captures a simple measure of seismic activity—the number of earthquakes in a certain magnitude range, without weighting them according to magnitude. Knopoff et al. (1996) explored N's individual performance for California. A particular feature of this measure is that it does not depend much on the relatively stronger and less numerous earthquakes.

Concentration of the main shocks in space (Z) Z is estimated as the ratio of the average diameter the earthquake sources to the average distance between them. This pattern was first found in the classical laboratory experiments of Zhurkov (1968).

Deviation of seismic activity from the long-term trend (L) *L* captures the increasing rate of the growth of seismic activity.

Time interval during which a given number of earthquakes occurred (R) A rise of activity is obviously indicated by a decrease of *R* (Shreider 1999). An unusual feature of that pattern is that count of time is replaced by count of earthquakes, as in the studies of acoustic emission.

Note on seismic quiescence Several studies report premonitory decrease of seismic activity (Shreider 1999, Wyss & Habermann 1987). This is not a contradiction because the rise and fall of activity may take place in different spatio-temporal scales (e.g., see Kossobokov et al. 1990) or succeed each other. For example, switching from low to high activity is one of the patterns used in the composite algorithm CN (Keilis-Borok & Rotwain 1990).

RISE OF EARTHQUAKE'S CLUSTERING

Burst of aftershocks or "Pattern B" Pattern *B* is captured by a main shock in a medium magnitude range with a large number of aftershocks in the first few days. Molchan et al. (1990) established high statistical significance of prediction by this pattern for 13 regions worldwide.

Swarm (S) *S* is a space-time cluster of main shocks with nearly the same magnitudes. Predictive power of this pattern is demonstrated for Italy, California and Nevada, Japan, and New Zealand (Keilis-Borok et al. 1980, Caputo et al. 1983).

Pattern BG This pattern is a cluster of earthquakes, aftershocks included, regardless of their magnitudes (Gabrielov et al. 1983). The remarkable feature of this pattern is that the magnitude should be known only for strong earthquakes, targeted for prediction. (Pattern *BG* was originally designed to use a regional catalog, containing only macroseismic intensities but not magnitudes of earthquakes.)

RISE OF EARTHQUAKE CORRELATION RANGE Premonitory seismicity patterns of this type recently attracted wide interest, and we give them a little more attention here.

Long-range aftershocks (LRA) *LRA* capture the earthquakes that occur immediately after a strong main shock at a large distance from the latter. According to Prozorov & Shreider (1990), such earthquakes form a long-term premonitory seismicity pattern: They occur near the epicenter of a future strong earthquake, to be expected within 10 years or so.

The two following patterns were found first in synthetic seismicity generated by the Colliding Cascades model (Gabrielov et al. 2000) and then in observations.

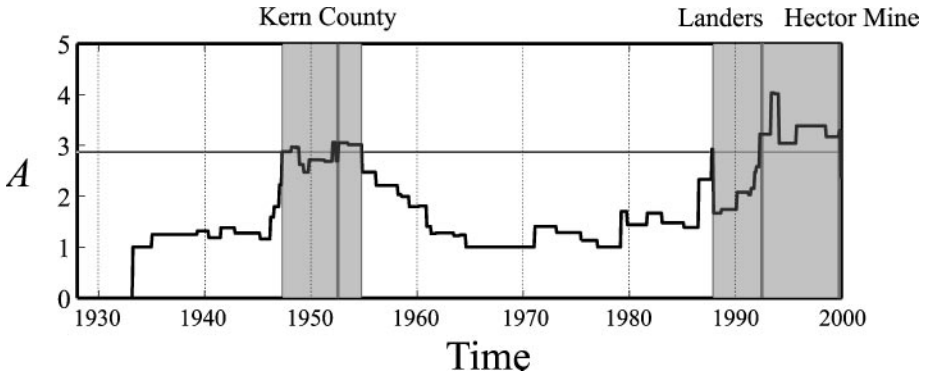

Figure 9 Performance of premonitory pattern Accord in Southern California (retrospective analysis). Function $A(t)$ depicts emergence of the pattern Accord. The alarms are shown in gray; the horizontal black line represents the threshold for declaring an alarm; vertical black lines show times of the three largest earthquakes. Function A obviously increases prior to these earthquakes. This result is stable to variations of adjustable elements of the prediction algorithm.

Pattern "Accord" This pattern is a nearly simultaneous activation of several major fault zones in the region, hence its name. Pattern *Accord* links the geometry of the fault network with universal (not Earth-specific) features of seismicity. Figure 9 shows its highly encouraging, albeit retrospective, application to Southern California (Zaliapin et al. 2000). That region comprises seven commonly recognized major fault zones. Seismic activity in each zone was measured by the total area of ruptures in seismic sources (as in pattern Σ). Scaled at predicting the earthquakes with $M > 7.5$, the pattern *Accord* emerges prior to the three largest earthquakes of the region: Kern County, in 1952; Landers, in 1992; and Hector Mine, in 1999, and at no other times. Rescaled at the lower target magnitudes, $6.5 \leq M < 7.5$, the pattern precedes six out of nine strong earthquakes, with the total duration of alarms 28% of the time considered. Predictions yield acceptable success-to-failure scores in a wide range of adjustable elements of the algorithm.

Pattern ROC (radius of correlation) Pattern *ROC* captures the nearly simultaneous occurrence of medium magnitude earthquakes at a large distance. Its successful (also retrospective) application to Lesser Antilles is described by Shebalin et al. (2000). A promising feature of this pattern is a higher accuracy of time-prediction; the duration of alarm is only a few months.

Distribution of links The distribution of links in a single-link cluster that connects epicenters of consecutive earthquakes was explored for seismicity of Southern California by Zoeller et al. (2001).

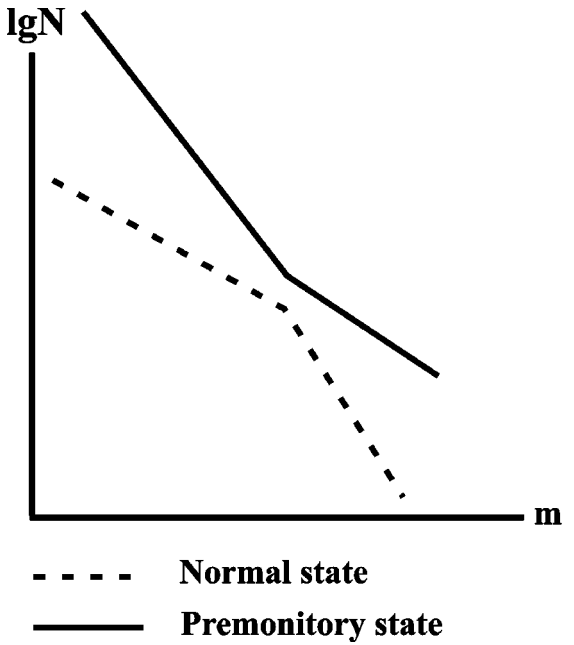

Figure 10 Premonitory changes of the Gutenberg-Richter relation. *N* is the occurrence rate of earthquakes, *m* is the magnitude (logarithmic measure of energy). The dashed line represents time far from a strong earthquake; the solid line represents time close to it.

CHANGE OF THE MAGNITUDE DISTRIBUTION The relation between the occurence rate N and the energy E of earthquakes is a fundamental feature of the dynamics of seismicity commonly known as the Gutenberg-Richter relation. It is often regarded as a power-law, which is actually an approximation valid only after a substantial averaging over time and territory, and within a limited energy range. Considering that relation in consecutive time intervals, one might see temporal variations preceding a strong earthquake. Two premonitory patterns of that type are schematically shown in Figure 10.

Upward bend (U) U captures the upward bend of the right-hand end of the $N(m)$ curve. Such a bend shows that relatively strong earthquakes gained a larger share of the whole seismicity. This pattern was first reported in laboratory experiments. Narkunskaya & Shirman (1994) analyzed the pattern in seismicity generated by a lattice-type hierarchical model of fracture development, and, in less detail, in observations.

Change of convexity (γ) This was first found in laboratory experiments with steel samples and then in observations for Southern California (Rotwain et al. 1997).

IRREGULARITY OF THE EARTHQUAKE SEQUENCE

Variation of magnitudes This is one of the patterns used jointly in algorithm SSE for predicting the second strong earthquake in a pair (see Composite Prediction Algorithms).

REVERSAL OF TERRITORIAL DISTRIBUTION OF SEISMICITY

Seismic reversal (SR) *SR* is the only pattern of this type so far suggested. It consists of the rise of activity on the faults, where average seismicity is relatively low, and, vice versa, drop of activity on the relatively active faults. This pattern was found in seismicity of Lesser Antilles (Shebalin & Keilis-Borok 1999).

CONCLUSION The above list is by no means complete, but well illustrates the multitude of reproducible premonitory seismicity patterns. Why should we consider such a multitude for earthquake prediction?

First, a set of patterns, even if correlated by definition, is more reliable than a single one, due to the complex nature of seismicity and unavoidable noise (Zaliapin et al. 2001). Second, a still unknown scenario of the development of a strong earthquake might include the advent of several independent phenomena. In that case, regardless of errors, an ensemble of phenomena might yield a better prediction. For these reasons, the composite prediction algorithms, using several premonitory patterns, are designed.

Composite Prediction Algorithms

Composite algorithms use a combination of individual precursors. Here we describe four such algorithms, relatively better validated by advance prediction in many regions worldwide.

ALGORITHM M8 This algorithm was designed by retrospective analysis of seismicity preceding the greatest ($M \geq 8$) earthquakes worldwide, hence its name. We describe it using as an example the recent prediction of major earthquake in Southern Sumatera, Indonesia, on June 4, 2000, $M = 8.0$. That prediction was part of the Russian-American experiment in advance prediction of strongest earthquakes worldwide. Figure 11 illustrates how this experiment works. The area targeted for prediction covers 80% of the major seismic belts—the territory for which earthquake catalog is sufficiently complete to apply the algorithm. This territory is scanned by overlapping circles with diameter of $12^\circ \approx 1333$ km. Prediction is made separately for each circle. Figure 11 shows alarms issued in January 2000, to be updated in six months.

The algorithm for issuing alarms is illustrated in Figure 12. It shows a case history of prediction of the Southern Sumatera earthquake. Three circles close to the epicenter of that earthquake are shown in Figure 12. Within each circle several characteristics of seismicity are estimated. Three characteristics, number of earthquakes (N), concentration of sources (Z), and deviation from long-term

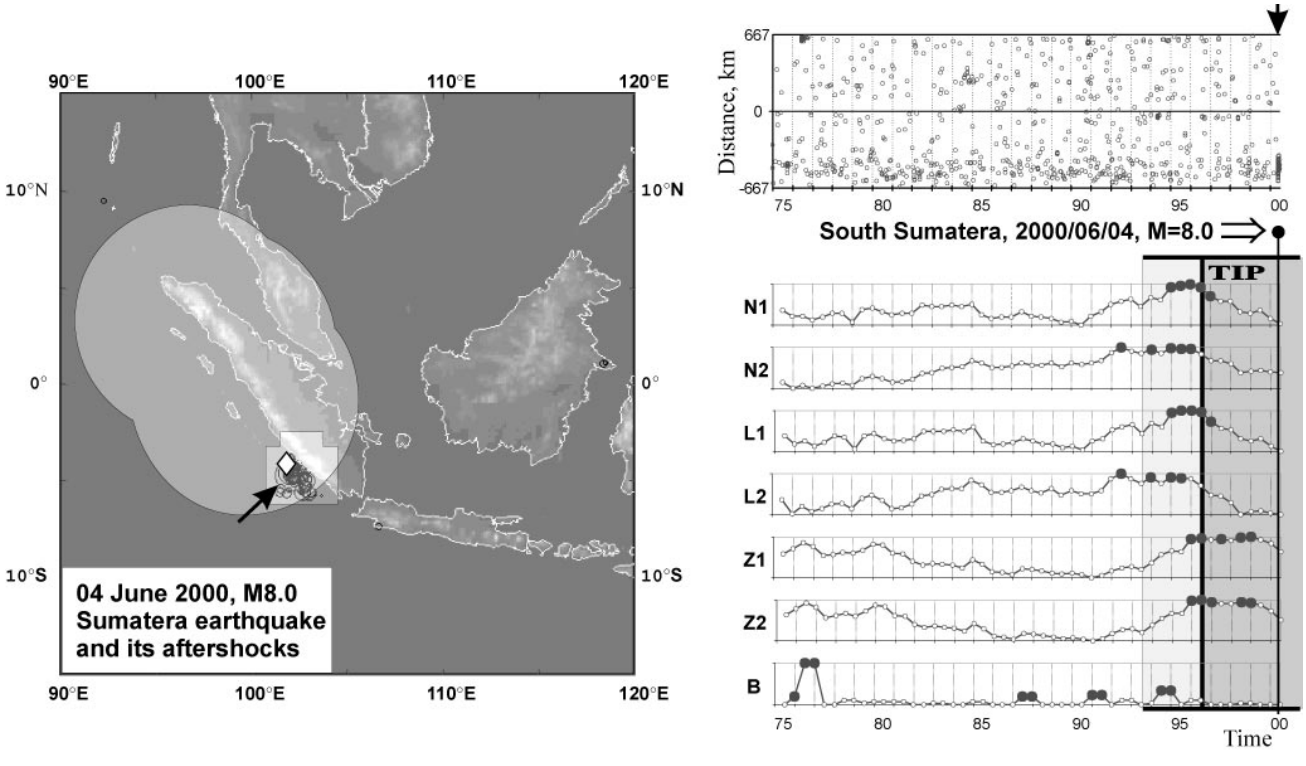

Figure 12 Advance prediction of the Southern Sumatera earthquake, June 4, 2000, M = 8.0. *Large light circles*—M8 alarms; *rectangular area*—MSc alarm; *black circles*—epicenters of the Sumatera earthquake and its aftershocks; *white diamond*—epicenter of a large foreshock, M = 4.7. Seismicity preceding the earthquake and functionals used for prediction are shown at the right; arrows show the time of the major earthquake. After Romashkova & Kossobokov 2001.

trend (L), depict seismic activity averaged over a large time window (six years); each is computed in two magnitude intervals to make description of seismicity more complete. One characteristic (B) depicts earthquake clustering. An alarm, or TIP, is issued for five years when clustering, and at least five other characteristics become "very large" at approximately the same time.

The alarm shown in Figure 12 appeared as early as July 1, 1996, with expiration on June 30, 2001. Four years after the onset of that alarm, on June 4, 2000, an earthquake of magnitude 8.0 occurred in S. Sumatera; its epicenter is shown on Figure 12 by a black circle; smaller circles show the aftershocks, roughly outlining the earthquake source. We see that the prediction was correct: This earthquake occurred within the territory and time-period covered by the alarm. The polygon in Figure 12 shows the smaller area of alarm; it is determined in a second approximation by the algorithm MSc (see below).

ALGORITHM MSc ("MENDOCINO SCENARIO") This algorithm was developed by retrospective analysis of seismicity prior to the Eureka earthquake (1980, $M = 7.2$) near Cape Mendocino in California, hence its name (Kossobokov et al. 1990). It is aimed at the reduction of the territory where a strong earthquake is already predicted by some other algorithm. Seismic activity in the territory of the original alarm is analyzed in more details. The alarm is confined to the area where seismicity is high but irregular, interrupted by short intervals of quiescence.

ALGORITHM CN The algorithm CN was developed (Keilis-Borok & Rotwain 1990) by retrospective analysis of seismicity preceding the earthquakes with $M \geq 6.5$ in California and the adjacent part of Nevada, hence its name. In that algorithm, seismicity is described by nine functionals, depicting seismic activity, its temporal variation, and bursts of aftershocks. Only large, medium, and small values of each function are distinguished. Qualitatively, an alarm starts when earthquake clustering is high; seismicity is irregular, high, and growing; and the increase of seismicity was preceded by quiescence.

ALGORITHM SSE (SECOND STRONG EARTHQUAKE) This algorithm was developed by retrospective analysis of 21 strong earthquakes in California and Nevada (Vorobieva & Levshina 1994). It is aimed at the following problem: A strong earthquake with magnitude M occurred and the beginning of its aftershock sequence is given; to predict whether a second strong earthquake, with magnitude $(M - 1)$ or larger, will occur within a certain distance $R(M)$ from the first one during T months thereafter (in practice $T = 18$ months).

Prediction is based on several characteristics of the aftershocks' sequence, depicting its intensity, irregularity, and territorial spreading. In addition, the algorithm uses activity preceding the first earthquake. This algorithm is applied to the nine regions shown in Figure 13. The choice of regions is restricted for the following reasons: First, the algorithm does not succeed in Circum-Pacific

subduction zones, reminding us that the similarity of premonitory phenomena is not unlimited; second, in many regions, the available earthquake catalogs are insufficiently complete.

Case history The first strong earthquake in that case was the Landers earthquake in Southern California, in 1992, M = 7.6. The map in Figure 14 shows the epicenters of this earthquake and its aftershocks. Algorithm SSE predicted that a second strong earthquake, M ≥ 6.6, would occur within 18 months after the Landers earthquake at the distance 200 km from its epicenter (Levshina & Vorobieva 1992). The corresponding alarm expired on December 28, 1993. The Northridge earthquake with M = 6.8 occurred within the above distance on January 17, 1994,

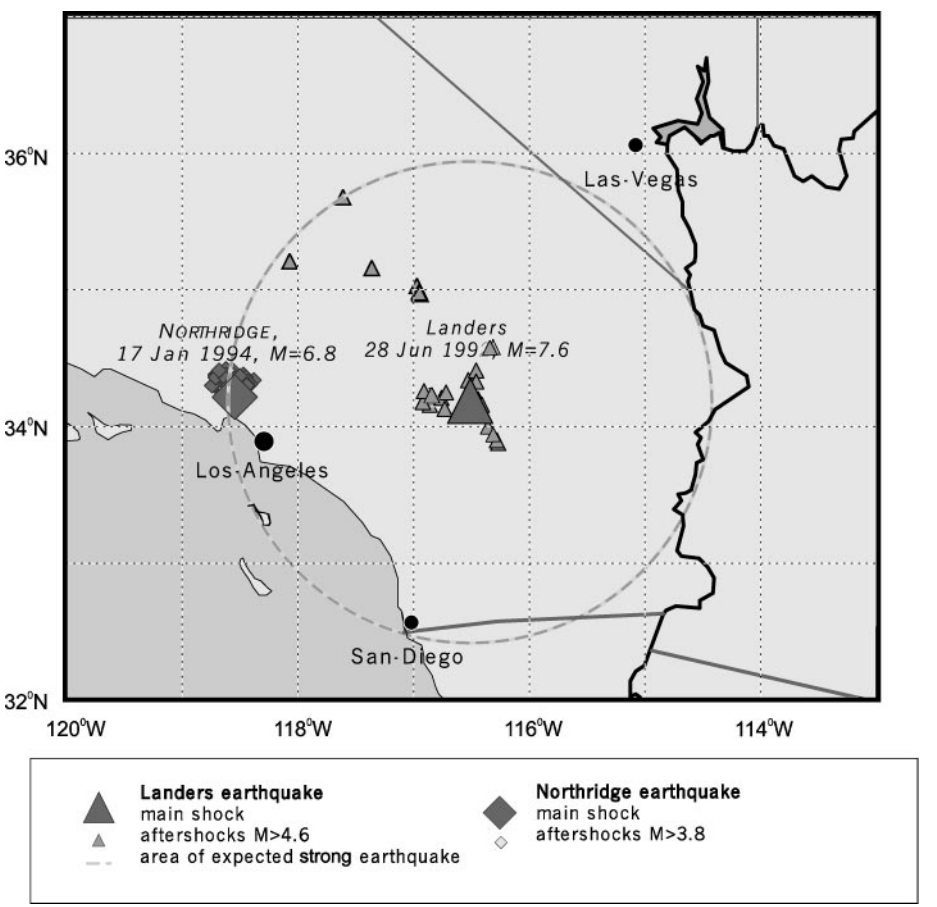

Figure 14 Advance prediction of the Northridge earthquake made by algorithm SSE. See details in the text. After Levshina & Verobieva 1992, Vorobieva 1999.

19 days after the expiration of the alarm; accordingly, this prediction is counted as a false alarm in the test of the algorithm. The algorithm SSE was then applied to the Northridge earthquake and generated no alarm. That prediction happened to be correct: no strong earthquakes occurred during the 18 months following the Northridge earthquake.

Importance Prediction of a second strong earthquake is specially important for several reasons: (*a*) The first earthquake can destabilize high-risk constructions and natural sources of hazard, like mountain slopes, glaciers, etc. (*b*) Disaster management services are already on the spot and need to know whether to relax or maintain safety measures (e.g., whether to let people return to their homes). (*c*) Public expectations are higher than for prediction in general: Failure to predict the first earthquake might be met with fatalism, but once it has happened, attention is riveted on the scientific community.

Advanced Prediction Worldwide

Here we describe the results of testing the composite algorithms, M8, MSc, and SSE, by advance prediction. We consider these algorithms because testing is continuing; recently, the predictions have been filed on a web site. The complete track record of the predictions, errors included, are available at http://www.mitp.ru or http://www.phys.ualberta.ca/mirrors/mitp.

ALGORITHMS M8 AND MSc The performance of algorithms M8 and MSc (Kossobokov et al. 1999) in predicting major earthquakes, with magnitude 8.0+ worldwide, is summed up in Table 2. Algorithm M8 successfully predicted all six strong earthquakes that occurred from 1992–2000. Algorithm MSc predicted five more accurately and missed one.

ALGORITHM SSE The performance of algorithm SSE (Vorobieva 1999) is summed up in Table 3. Advance prediction started in 1989. Up to the year 1998, 20 strong

TABLE 2 Performance of the prediction algorithms M8 and MSc for earthquakes of magnitude 8.0 and more. After (Kossobokov et al. 1999)*

Test period	Strong earthquakes	Predicted by		Space-time covered by alarms, %	
		M8	MSc	M8	MSc
1985–2000	8	8	7	34.9	18.0
1992–2000	6	6	5	30.2	15.3

*Data for the period 1997–2000 are taken from http://www.mitp.ru (mirror at http://www.phys.ualberta.ca/mirrors/mitp).

TABLE 3 Performance of the prediction algorithm SSE. After (Vorobieva 1999)

		Did a subsequent strong earthquake occur?			
PREDICTIONS:		**YES**		**NO**	
Test period	**Strong earthquakes**	**Total**	**Correct**	**Total**	**Correct**
1989–1998	20	6	4	14	13

earthquakes occurred and 6 of them were followed by a second strong earthquake; the algorithm made 17 correct predictions and 3 mistakes.

EARTHQUAKE PREDICTION AND EARTHQUAKE PREPAREDNESS

Currently realistic earthquake predictions have limited accuracy. How can one use them to reduce damage from the earthquakes? The key is to escalate or de-escalate preparedness depending on (*a*) the content of a current alarm (what is predicted and where); (*b*) the probability of a false alarm; and (*c*) the cost/benefit ratio of disaster-preparedness measures. Such is the standard practice in preparedness for all disasters, war included. A costly mistake—that only a precise short-term prediction is practically useful (besides estimation of seismic hazard)—emerges from time to time in the seismological literature. Actually, as in the case of defense, prediction may be useful if its accuracy is known, even if it is not high.

Diversity of Damage

Earthquakes may destroy buildings, lifelines, etc.; trigger fires; release toxic, radioactive, and genetically active materials; and trigger floods, avalanches, landslides, tsunamis, etc. Equally dangerous are the socio-economic and political consequences of earthquakes: disruption of vital services—supply, medical, financial, law enforcement, etc.; epidemics; of production and unemployment; military destabilization; profiteering, crime, and disruptive anxiety of population. The socio-economic consequences may be inflicted also by the undue release of predictions.

Disaster Preparedness Measures

Such diversity of damage requires a hierarchy of disaster-preparedness measures, from building codes and insurance to mobilization of post-disaster services to a red alert. It takes different times, from decades to seconds, to undertake different measures; having different costs, they can be maintained for different time periods.

Accordingly, no single stage can replace another one for damage reduction, and no single measure is sufficient alone.

Many important measures do not require a particularly precise prediction. An example is the 1994 Northridge earthquake, California, mentioned above, which caused economic damage on the order of $30 billion. Its prediction, published well in advance (Levshina & Vorobieva 1992), was not precise: The alarm covered an area 400 km in diameter and time period of 18 months. However, an inexpensive, low-key response to this prediction (e.g., out-of-turn safety inspection) would be well justified if even a few percent of the damage is prevented.

Optimization

The framework for the optimal choice of disaster-preparedness measures undertaken in response to an alarm was developed by Molchan (1997); earlier analysis of the problem is described in (Kantorovich & Keilis-Borok 1991). Optimization is based on the error diagrams and the trade-off between cost and benefits of different measures.

WHAT COMES NEXT?

Expansion of Observational Base

Yet unknown precursors may exist in a wealth of observed fields potentially relevant to earthquake prediction: stress and strain, slow tectonic movements, satellite topography, fluid regimes, geochemistry, electric and magnetic fields, etc. It seems promising to explore such precursors with the common scaling and common types of premonitory phenomena—similar to those found for premonitory seismicity patterns.

Precursors Specific to Tectonic Environment

The search for precursors specific to the tectonic environment includes premonitory changes in geometric and kinematic incompatibilities; different precursors in the nodes, fault zones, and blocks; and, finally, region-specific precursors. Valuable for the last purpose is a rich collection of errors and successful predictions in more than 20 regions worldwide (Keilis-Borok & Shebalin 1999).

Scenarios of Transition to a Strong Earthquake

There is evidence that premonitory seismicity patterns appear in a certain order depending on the type of the pattern and on its scaling in time, space, and magnitude range. This experience suggests that different precursors—not necessarily only seismological—might be integrated in a unified scenario of development of a strong earthquake, extending through consecutive stages of prediction.

Conclusion

Altogether, these lines of research are converging on the following goals, which seem marginally feasible: development of the next generation of prediction algorithms, 5- to 10-times more accurate than existing ones; prediction of earthquakes in low seismicity regions with rare devastating earthquakes; and prediction of geotechnical and other geological disasters.

ACKNOWLEDGMENTS

Dr. I. Zaliapin made a large and important contribution to work for this review. My colleagues from the International Institute of Earthquake Prediction Theory and Mathematical Geophysics, Moscow, willingly provided invaluable original materials of their research.

LITERATURE CITED

Aki K. 1996. Scale dependence in earthquake phenomena and its relevance to earthquake prediction. *Proc. Natl. Acad. Sci. USA* 93:3748–55

Alekseevskaya M, Gabrielov A, Gelfand I, Gvishiani A, Rantsman E. 1977. Formal morphostructural zoning of mountain territories. *J. Geophys.* 43:227–33

Barenblatt GI, Keilis-Borok VI, Monin AS. 1983. Filtration model of earthquake sequence. *Dokl. Akad. Nauk SSSR* 269(4):831–34 (In Russian)

Bowman DD, Ouillon G, Sammis CG, Sornette A, Sornette D. 1998. An observational test of the critical earthquake concept. *J. Geophys. Res.* 103:24359–72

Bufe CG, Varnes DJ. 1993. Predictive modeling of the seismic cycle of the greater San Francisco bay region *J. Geophys. Res.* 98:9871–83

Caputo M, Console R, Gabrielov AM, Keilis-Borok VI, Sidorenko TV. 1983. Long-term premonitory seismicity patterns in Italy. *Geophys. J. R. Astron. Soc.* 75:71–75

Crutchfield JP, Farmer JD, Packard NH, Shaw RS. 1986. Chaos. *Sci. Am.* 255:46–57

Gabrielov A, Keilis-Borok VI, Jackson DD. 1996. Geometric incompatibility in a fault system. *Proc. Natl. Acad. Sci. USA* 93(9): 3838–42

Gabrielov AM, Caputo M, Keilis-Borok VI, Console R, Sidorenko TV. 1983. Long-term premonitory seismicity patterns in Italy. *Geophys. J. R. Astron. Soc.* 75:71–75

Gabrielov AM, Keilis-Borok VI. 1983. Patterns of stress corrosion: geometry of the principal stresses *Pure Appl. Geophys.* 121:477–94

Gabrielov AM, Zaliapin IV, Newman WI, Keilis-Borok VI. 2000. Colliding cascades model for earthquake prediction. *J. Geophys. Int.* 143:427–37

Gelfand IM, Guberman ShA, Keilis-Borok VI, Knopoff L, Press F, et al. 1976. Pattern recognition applied to earthquake epicenters in California. *Phys. Earth Planet. Inter.* 11:227–83

Gell-Mann M. 1994. *The Quark and the Jaguar: Adventures in the Simple and the Complex.* New York: Freeman

Gorshkov AI, Kossobokov VG, Rantsman EYa, Soloviev AA. 2001. Recognition of earthquake prone areas: validity of results obtained from 1972 to 2000. *Vych. Seism.* 32:48–57

Holland JH. 1995. *Hidden Order: How Adaptation Builds Complexity*. Reading, MA: Addison-Wesley

Kantorovich LV, Keilis-Borok VI. 1991. Earthquake prediction and decision-making: social, economic and civil protection aspects. In *Int. Conf. Earthquake Prediction: State-of-the-Art, Strasbourg, Fr., Sci.-Tech. Contrib., CSEM-EMSC*, pp. 586–93

Keilis-Borok VI. 1990a. The lithosphere of the Earth as a non-linear system with implications for earthquake prediction. *Rev. Geophys.* 28(1):19–34 (Transl. into Chinese)

Keilis-Borok VI, ed. 1990b. Intermediate-term earthquake prediction: models, phenomenology, worldwide tests. *Phys. Earth Planet. Inter.* 61:1–144

Keilis-Borok VI, Knopoff L, Rotwain IM. 1980. Bursts of aftershocks, long-term precursors of strong earthquakes. *Nature* 283:258–63

Keilis-Borok VI, Kossobokov VG. 1990. Premonitory activation of earthquake flow: algorithm M8. *Phys. Earth Planet. Inter.* 61:73–83

Keilis-Borok VI, Malinovskaya LN. 1964. One regularity in the occurrence of strong earthquakes. *J. Geophys. Res.* 69(14):3019–24

Keilis-Borok VI, Press F. 1980. On seismological applications of pattern recognition. In *Source Mechanism and Earthquake Prediction Applications*, ed. CJ Allegre, pp. 51–60. Paris: Ed. Cent. Natl. Rech. Sci.

Keilis-Borok VI, Rotwain IM. 1990. Diagnosis of time of increased probability of strong earthquakes in different regions of the world: algorithm CN. *Phys. Earth Planet. Inter.* 61: 57–72

Keilis-Borok VI, Shebalin PN, eds. 1999. Dynamics of lithosphere and earthquake prediction. *Phys. Earth Planet. Inter.* 111:179–330

King GCP. 1983. The accommodation of large strain in the upper lithosphere of the Earth and other solids by self-similar fault systems: the geometrical origin of b-value. *Pure Appl. Geophys.* 121:761–815

Knopoff L, Levshina T, Keilis-Borok VI, Mattoni C. 1996. Increased long-range intermediate-magnitude earthquake activity prior to strong earthquakes in California. *J. Geophys. Res.* 101:5779–96

Kossobokov VG, Carlson JM. 1995. Active zone size vs. activity. A study of different seismicity patterns in the context of prediction algorithm M8. *J. Geophys. Res.* 100: 6431–41

Kossobokov VG, Keilis-Borok VI, Cheng B. 2000. Similarities of multiple fracturing on a neutron star and on the Earth. *Phys. Rev. E* 61(4):3529–33

Kossobokov VG, Keilis-Borok VI, Smith SW. 1990. Localization of intermediate-term earthquake prediction. *J. Geophys. Res.* 95: 19763–72

Kossobokov VG, Romashkova LL, Keilis-Borok VI, Healy JH. 1999. Testing earthquake prediction algorithms: statistically significant advance prediction of the largest earthquakes in the Circum-Pacific, 1992–1997. *Phys. Earth Planet. Inter.* 111:187–96

Levshina T, Vorobieva I. 1992. Application of algorithm for prediction of a strong repeated earthquake to the Joshua Tree and Landers earthquakes. *EOS, Trans. Am. Goephys. Union* 73:382

McKenzie DP, Morgan WJ. 1969. Evolution of triple junctions. *Nature* 224:125–33

McKenzie DP, Parker RL. 1967. The North Pacific: an example of tectonics on a sphere. *Nature* 216:1276–80

Molchan GM. 1997. Earthquake prediction as a decision-making problem. *Pure Appl. Geophys.* 149:233–47

Molchan GM, Dmitrieva OE, Rotwain IM, Dewey J. 1990. Statistical analysis of the results of earthquake prediction, based on burst of aftershocks. *Phys. Earth Planet. Inter.* 61:128–39

Narkunskaya GS, Shnirman MG. 1994. An algorithm of earthquake prediction. In *Computational Seismology and Geodynamics*, 1:20–24. Washington, DC: Am. Geophys. Union

Newman WI, Gabrielov A, Turcotte DL, eds. 1994. *Nonlinear Dynamics and Predictability of Geophysical Phenomena. Geophys.*

Monogr. Ser. 83. Washington, DC: Am. Geophys. Union

Newman WI, Turcotte DL, Gabrielov A. 1995. Log-periodic behavior of a hierarchical failure model with applications to precursory seismic activation. *Phys. Rev. E* 52:4827–35

Pepke GF, Carlson JM, Shaw BE. 1994. Prediction of large events on a dynamical model of fault. *J. Geophys. Res.* 99:6769–88

Press A, Allen C. 1995. Pattern of seismic release in the southern California region. *J. Geophys. Res.* 100:6421–30

Prozorov AG, Schreider SYu. 1990. Real time test of the long-range aftershock algorithm as a tool for mid-term earthquake prediction in Southern California. *Pure Appl. Geophys.* 133:329–47

Richter CF. 1964. Discussion of paper by VI Keilis-Borok and LN Malinovskaya, "One regularity in the occurrence of strong earthquakes." *J. Geophys. Res.* 69(14):3025

Romanowicz B. 1993. Spatiotemporal patterns in the energy-release of great earthquakes. *Science* 260:1923–26

Romashkova LL, Kossobokov VG. 2001. Seismicity dynamics prior to and after the largest earthquakes worldwide 1985–2000. *Vych. Seism.* 32:162–89

Rotwain I, Keilis-Borok V, Botvina L. 1997. Premonitory transformation of steel fracturing and seismicity. *Phys. Earth Planet. Inter.* 101:61–71

Rundle BJ, Turcotte DL, Klein W, eds. 2000. *Geocomplexity and the Physics of Earthquakes.* Washington, DC: Am. Geophys. Union

Shebalin P, Zaliapin I, Keilis-Borok V. 2000. Premonitory raise of the earthquakes' correlation range: Lesser Antilles. *Phys. Earth Planet. Inter.* 122:241–49

Shebalin PN, Keilis-Borok VI. 1999. Phenomenon of local "seismic reversal" before strong earthquakes. *Phys. Earth Planet Inter.* 111:215–27

Shreider SYu. 1999. Formal definition of premonitory seismic quiescence. *Phys. Earth Planet. Inter.* 61:113–27

Soloviev A, Vorobieva I. 1999. Long-range interaction between synthetic earthquakes in the model of block structure dynamics. *5th Workshop Non-Linear Dyn. Earthquake Prediction, 4–22 Oct.* Trieste: ICTP, Preprint H4. SMR/1150-4. 18 pp.

Sornette D. 2000. *Critical Phenomena in Natural Sciences. Chaos, Fractals, Self-organization and Disorder: Concepts & Tools.* Springer Ser. Synerg., Heidelberg. New York: Springer-Verlag. 432 pp.

Sornette D, Sammis CG. 1995. Complex critical exponents from renormalization group theory of earthquakes: implications for earthquake predictions *J. Phys. I* 5:607–19

Turcotte DL. 1997. *Fractals and Chaos in Geology and Geophysics.* Cambridge: Cambridge Univ. Press. 2nd ed.

Vorobieva IA. 1999. Prediction of a subsequent strong earthquake. *Phys. Earth Planet. Inter.* 111:197–206

Vorobieva IA, Levshina TA. 1994. Prediction of a second large earthquake based on aftershock sequence. In *Computational Seismology and Geodynamics*, 2:27–36. Washington, DC: Am. Geophys. Union

Wyss M, Habermann RE. 1987. Precursory seismic quiescence. Physical and observational basis for intermediate-term earthquake prediction. *US Geol. Surv. Open-File Rep.* 2:526–36

Zaliapin I, Keilis-Borok VI, Axen G. 2002. Premonitory spreading of seismicity over the fault network in S. California: precursor accord. *J. Geophys. Res.* In press

Zaliapin I, Keilis-Borok VI, Ghil M. 2001. Boolean delay model of colliding cascades. II: Prediction of critical transitions. *J. Stat. Phys.* Submitted

Zoeller G, Hainzl S, Kurths J. 2001. Observation of growing correlation length as an indicator for critical point behavior prior to large earthquakes. *J. Geophys. Res.* 106:2167–76

Zhurkov SN. 1968. Kinetic concept for strength of solids. *Vestn. Akad. Nauk SSSR* 3:46–52

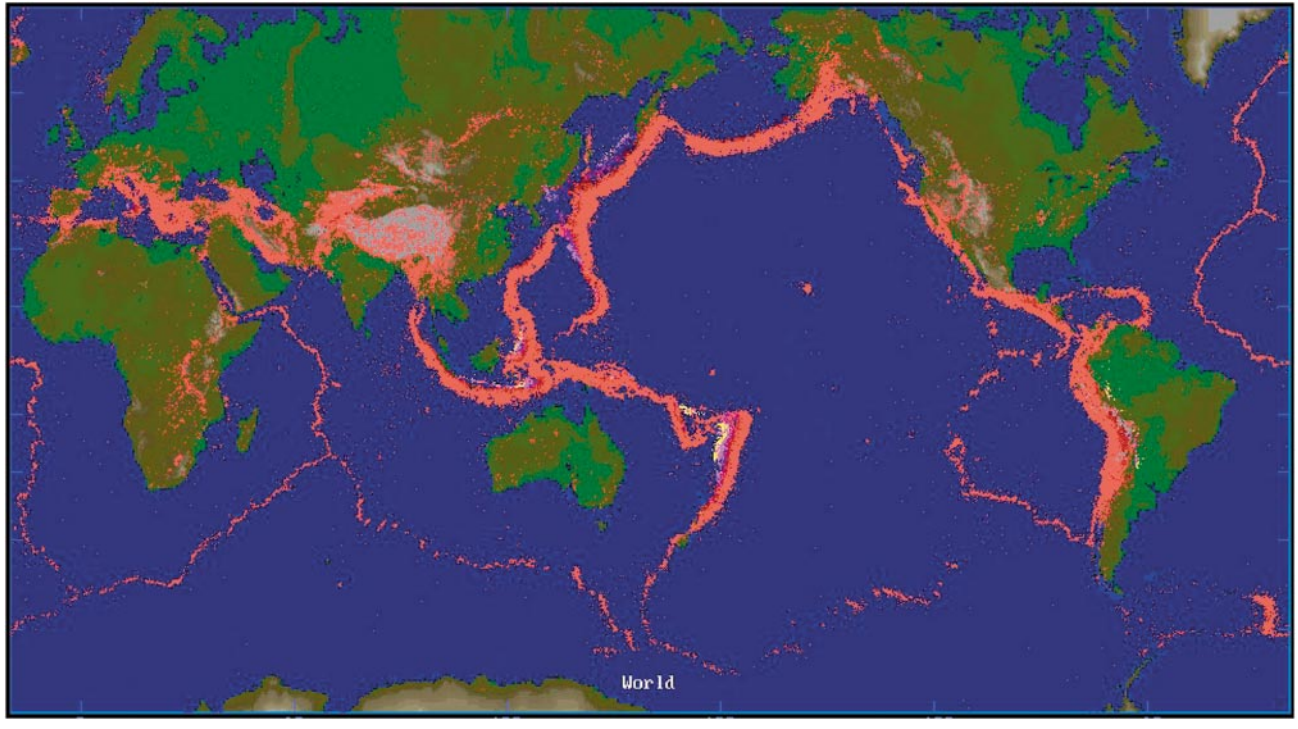

Figure 1 Global distribution of seismicity. *Red* points show earthquakes with magnitude greater than 4.0 for the last century. They clearly outline the global fault network. From http://www.mitp.ru.

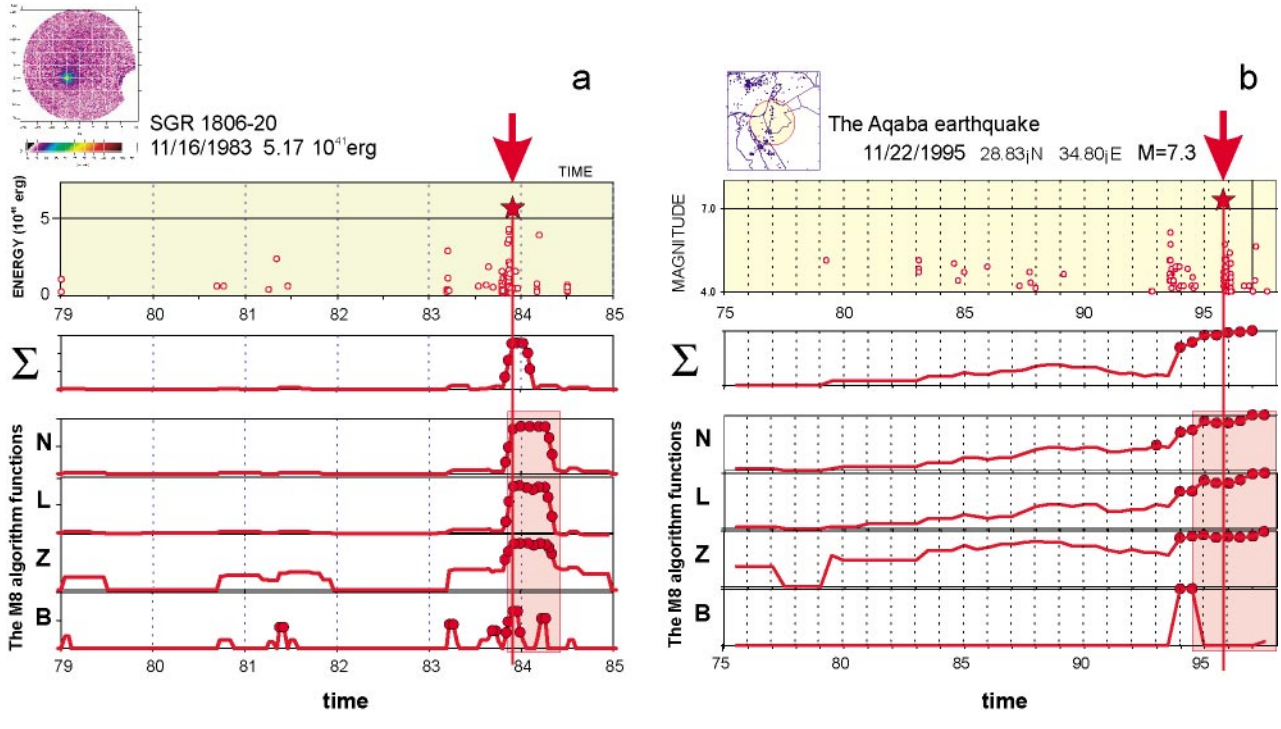

Figure 8 Frontier of similarity of premonitory seismicity patterns. (*a*) Starquake, registered on November 16, 1983; magnitude is approximately 20. (*b*) Aqaba earthquake, November 22, 1995; M = 7.3. *Top panels*: sequence of starquakes (*left*) and earthquakes (*right*). Stars indicate the major events, targeted for prediction. Other panels show the emergence of different premonitory seismicity patterns; note that they have been developed for seismicity of the Earth only. *B* is the measure of clustering, other functionals are different measures of seismic activity (see Prediction). *Solid dots* indicate emergence of a premonitory pattern. After Kossobokov et al. 2000.

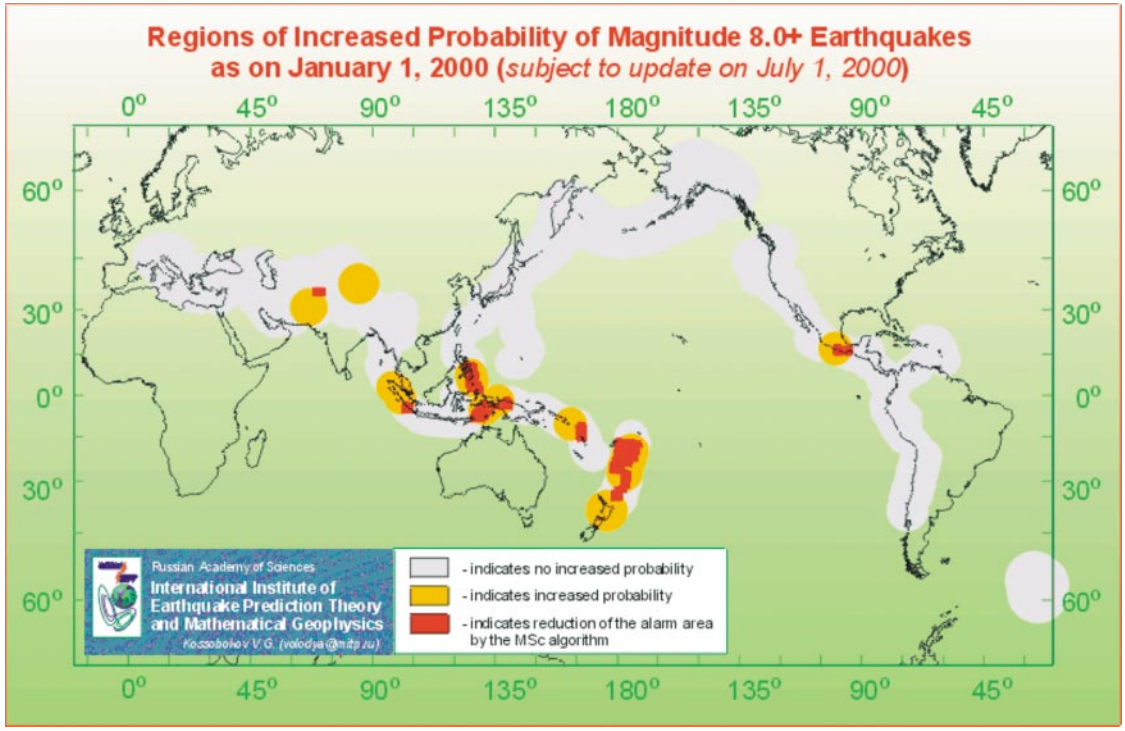

Figure 11 Global prediction issued by algorithm M8 in January, 2000. *Gray*—territory targeted for prediction; *yellow*—alarms by the algorithm M8; *red*—alarms by the algorithm MSc. See details in the text. From http://www.mitp.ru (mirror at http://www.phys.ualberta.ca/mirrors/mitp).

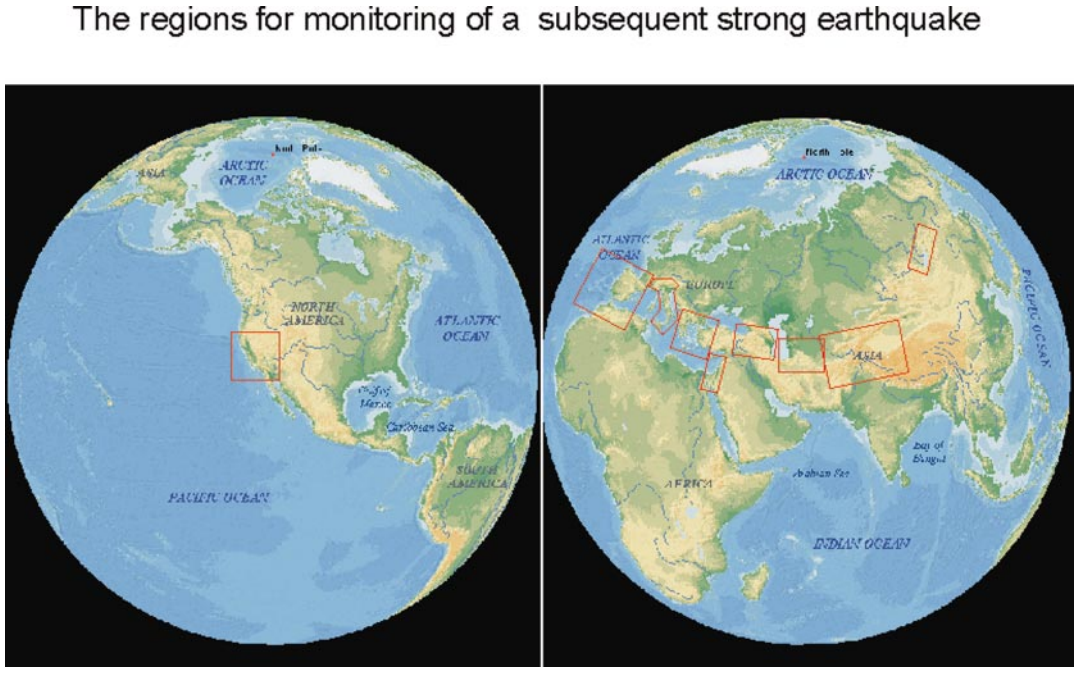

Figure 13 Regions targeted for prediction by algorithm SSE (second strong earthquake). Taken from http://www.mitp.ru (mirror at http://www.phys.ualberta.ca/mirrors/mitp).